JOURNAL OF SPACECRAFT AND ROCKETS
Vol. 39, No. 5, September–October 2002

Geometric Imperfection Effects in an Elastically Deployable Isogrid Column

Jason D. Hinkle*
University of Colorado, Boulder, Colorado 80309
Peter Warren†
Foster Miller, Inc., Waltham, Massachusetts 02154
and
Lee D. Peterson‡
University of Colorado, Boulder, Colorado 80309

The experimental study and analysis of a novel gossamer structural component is described. The component is a 3-m-long thin-walled isogrid column prototype that may be elastically stowed and deployed. The column has a diameter of 0.318 m, with a linear density of 46 g/m. The static and dynamic mechanical responses of the deployed prototype are examined and compared to an idealized model. These comparisons indicate global stiffness ranging from 11 to 28% and buckling strengths from 7 to 37% of the theoretically ideal performance. Initial local curvatures approaching the thickness of the isogrid ribs are found to be the primary source of this performance reduction. A modeling approach based on the postbuckled response of individual isogrid ribs is proposed for predicting the global effects of local imperfections, and good agreement with the test results is found. In general, initial rib curvatures greater than 10% of the rib thickness are predicted to result in significant degradations of the global structural performance.

Nomenclature

A	=	cross-sectional area, m^2
b	=	isogrid rib width, m
c	=	compliance, m/N
E	=	Young's modulus, Pa
f	=	vibration frequency, rad/s
h	=	isogrid rib spacing, m
I	=	minimum rectangular moment of inertia, m^4
J	=	rotational inertia, $kg \cdot m^2$
k	=	stiffness, N/m (or Nm/rad)
L	=	length, m
P	=	axial load, N
q	=	normalized axial load
r	=	column radius, m
t	=	column/rib thickness, m
γ	=	knockdown factor
δ	=	axial deflection, m
ε	=	imperfection amplitude, m
σ	=	stress, N/m^2
ϕ	=	thin-walled cylinder exponent

Subscripts

axial	=	axial properties
bending	=	bending properties
cr	=	critical load
eff	=	effective properties
ideal	=	ideal properties
rib	=	individual rib properties
torsion	=	torsion properties
wall	=	isogrid wall properties

Received 18 June 2001; revision received 4 March 2002; accepted for publication 18 April 2002.

*Research Associate, Center for Aerospace Structures, Department of Aerospace Engineering Sciences. Member AIAA.
†Senior Engineer, Structures and Transportation Division. Member AIAA.
‡Associate Professor, Center for Aerospace Structures, Department of Aerospace Engineering Sciences. Associate Fellow AIAA.

Introduction

NASA has, in the past decade, placed an increasing emphasis on the development of novel mission concepts and technologies to enable more aggressive missions with more limited budgets. Included in these has been a renewed interest in extraordinarily large and mass-efficient, or gossamer, structures. Proposed applications for these systems include large apertures for science instruments, solar concentrators for propulsion, and solar sails.

A common structural challenge in many of these systems is the need for equally long and mass-efficient beam columns for the transfer of compressive and bending loads. This requirement is exemplified by a number of missions currently under study. The Solar Electric Transfer Vehicle being investigated by the NASA John H. Glenn Research Center at Lewis Field would utilize two photovoltaic arrays deployed and supported by 95-m long columns.[1] The Advanced Radio Interferometry between Space and Earth mission requires a 25-m-diam inflatable antenna with approximately 20-m support columns. The National Oceanographic and Atmospheric Administration and NASA are designing the Geostorm mission to provide early warning of solar events. The baseline design would use a solar sail to maintain an otherwise unstable orbit between the Earth and the sun. A technology development mission proposed for this program would deploy a 100-m-class solar sail using 70-m-long columns to deploy and tension the sail film. More aggressive solar sail mission concepts for interplanetary and even interstellar exploration demand significantly larger and more efficient structural systems.

Simultaneously satisfying the scale, efficiency, and stability requirements for these structural components presents one of the challenges of gossamer spacecraft design. Thin-walled monocoque columns provide one solution with high bending stiffness-to-mass ratios and the packaging efficiency of inflatables. However, as the scale increases and loads are reduced, the wall thickness of these designs limits their practical performance. Specifically, as the wall thickness decreases, local imperfections introduced by fabrication and handling greatly reduce the effective strength of the component. A discussion of the experimental and analytical study of the buckling of thin-walled cylinders is provided in Ref. 2.

Another study, focused on long, lightly loaded columns, presented a number of potential architectural solutions to this problem.[3] One such approach is to utilize an isogrid, rather than monocoque, wall architecture. This results in a concentration of wall material into thicker elements with greater tolerance for geometric imperfections while maintaining the structural efficiency of thin-walled circular cylinders.

Motivated by the preceding considerations, a manufacturing technique for a deployable thin-walled isogrid column has been developed. A prototype from this process was constructed to determine initial levels of performance and to suggest improvements in the fabrication process. The individual ribs of this structure are designed to permit the column to be elastically stowed.

This paper reports on an experimental and analytical investigation of this prototype. The stiffness and strength of the column is found to be limited by geometric imperfections at the individual rib level resulting from fabrication and test fixturing. To allow the column to be elastically stowed, the ribs are relatively slender and, therefore, sensitive to small initial curvatures. The relationship between these local imperfections and the column's global stiffness and strength is, therefore, the focus of this investigation.

A significant amount of previous work with isogrid systems is available in the literature. Particular attention has been paid to isogrid-stiffened plates and shells.[4] One of the benefits of isogrid systems is their generally isotropic behavior, and modeling these systems with equivalent isotropic material properties has proven effective. This trait permits the application of a range of stiffness and stability analyses previously derived and verified for monocoque plates and shells.

However, the accuracy of such simplified analyses is uncertain as the scales of deformation, that is, buckled mode shapes, approach that of the grid spacing.[3,4] At this scale, more detailed analyses are required. Reference 3 presents strength-based design analyses for both solid rod and tubular truss columns. Whereas these analyses considered local member and global Euler buckling limitations, other truss analyses addressed the more general buckling of periodic lattice structures.[5,6] Note that a great deal of additional work has been done in the analysis of the stiffness and strength of related truss and frame systems that is beyond the scope of the current study.

As with thin-walled monocoque systems, the influence of geometric imperfections on isogrid systems can be significant. In a 1982 paper, Anderson comments that "the very light loadings and large dimensions expected for space application will lead to very flexible members and require accurate analysis to assure structural integrity. In many cases imperfections in members with large slenderness ratios will be an important design consideration."[7]

Again, a significant amount of previous study of imperfection effects is available. Analytical and experimental studies of imperfect beam columns have been performed.[8–10] These studies generally confirmed the applicability of the classical Euler beam column theories and demonstrated the sensitivity of such testing to specimen geometry and experimental methods. Analyses of imperfection effects in lattice and truss structures have also been performed.[7,11–13]

An apparent gap in this previous work is the experimental study of imperfection effects in truss and open isogrid structures. Although experimental investigations of isogrid-stiffened plates and shells are fairly extensive, such studies of open isogrid systems appear to be more limited.[4] One likely reason for this is the difficulty of making sufficiently precise measurements of these imperfections. This lack of precision proved to be a limitation to the work described herein.

Along with a characterization of the gossamer isogrid column's structural performance, a new method of including rib imperfections in the analysis of open isogrid systems is proposed and applied here. The ribs are modeled as individual Euler beam columns with initial curvatures, and the resulting decreases in local stiffness are related to the global system through an equivalent elastic modulus approach. This model is used to relate the observed stiffness and strength reductions to the initial rib curvatures.

The amplitude and distribution of rib curvatures inferred from the model are found to agree with measurements of the initial imperfections. In particular, a three order of magnitude knockdown factor for the column's torsional stiffness is measured. This knockdown factor is due to relatively large initial curvature in the diagonal ribs resulting from the prototype's fabrication process. The observed magnitude of this curvature corresponds to that predicted by the equivalent modulus model.

The remainder of the paper is organized as follows. The test article, experiment configuration, and testing procedures are first described. The structural performance under axial and bending loads and in torsional vibration is then presented. Finally, an analysis of the relationship between local rib imperfections and the global structural response is developed and compared with the data.

Experiment Configuration

The thin-walled isogrid column prototype being studied is shown in Fig. 1. The column is 0.318 m in diameter and 2.97 m in length, with a mass of 137 g. The isogrid material consists of 0.2-mm-thick × 2.3-mm-wide ribs with a rib-to-rib spacing of 56 mm. The ribs consist of a fiberglass–epoxy composite material with a measured axial modulus of 13 GPa. The bending compliance of the ribs allows the column to be elastically packaged into a 505-cm^3 volume.

To allow the column to be constrained, loaded, and instrumented, relatively stiff end fittings were attached. Given the compliance of the test article, one challenge was to avoid introducing detrimental local deformations of the column. To this end, an epoxy-based potting approach was selected, which allowed the end fittings to conform to the irregular rib locations. As shown in Fig. 2, rings of aluminum flashing were used to form a 6.4-mm-thick mold. At this point, the column axis and end fittings were aligned by leveling the assembly table and ensuring the column was hanging vertically (both to ± 0.2 deg). This alignment was critical to ensure the final orientation of the column with respect to gravity. Gap-filling epoxy was then injected into the mold and allowed to join the column and end fitting. As discussed later, the viscosity of the epoxy resulted in small ($\approx$1 mm), but significant rib deformations during the potting process. The likely future solution to this is to use a sealed mold design and a less viscous potting agent.

Unistrut® mounting brackets were added to allow the upper end to be fixed to an overhead frame. This end fitting was left open to allow access for an axial loading cable. The unconstrained lower end fitting included mounting hardware for load application and displacement measurement.

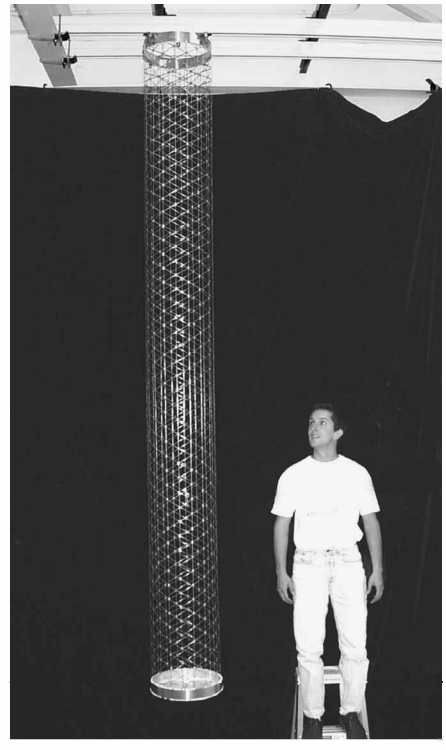

Fig. 1 Gossamer isogrid column test article.

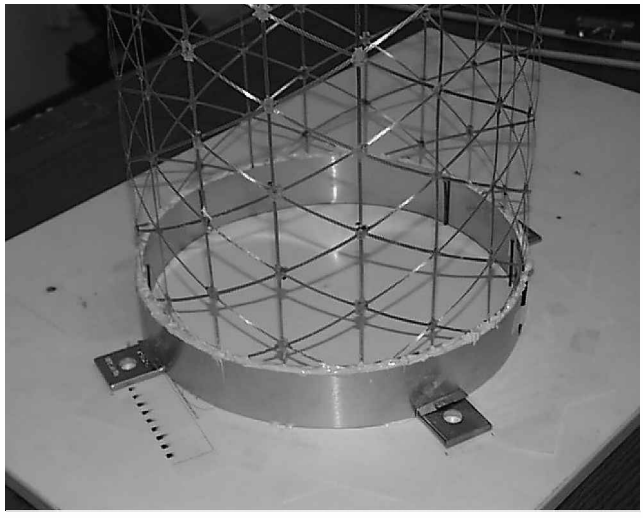

Fig. 2 End fitting assembly.

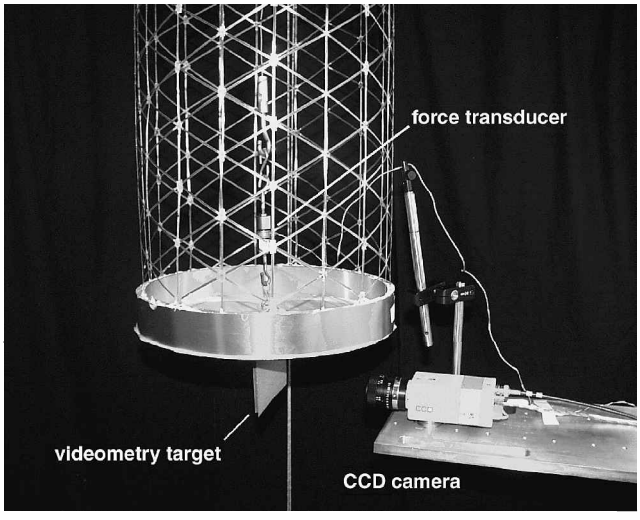

Fig. 3 Videometry system configuration.

A fixed–free boundary condition arrangement was selected for testing the 3-m column. The column was oriented vertically to simplify the control of gravitational loading effects (Fig. 1). This configuration allowed for the careful control of the initial stress state of the column. It also permitted both axial and bending loads to be applied beyond their respective buckling points.

A videometry system was used to observe axial and lateral motion of the free end of the column.[14] This noncontact metrology system permitted unhindered motion of the column and provided 10-μm resolution across 2 cm of axial and lateral travel. The location and orientation of the target and camera are shown in Fig. 3. Given the compliance of the test article, it was assumed that the deformation of the support structure was negligible.

Axial and lateral loads were applied to the free end using tension lines to limit unintended stiffness contributions. The pulley system shown in Fig. 4 was used to maintain the axial loading cable's alignment with the column's axis. The pulley over the column was positioned to center the cable along the column's axis to within ± 1 mm. Incremental loads were applied with weights and the resulting input load measured at the point of transmission to the column with a dc force transducer. This transducer had an absolute accuracy near 0.05 N.

Because of the low bending vibration frequency and damping of the test article, it was necessary to allow roughly 1 min for structural vibrations to damp out following the application of load increments. It was also necessary to shield the column from air drafts with a curtain placed within about a meter along the entire length. Load and displacement data were collected automatically, whereas the load increments were applied manually. When these procedures were followed, the repeatability of the data was found to approach the resolution of the instrumentation.

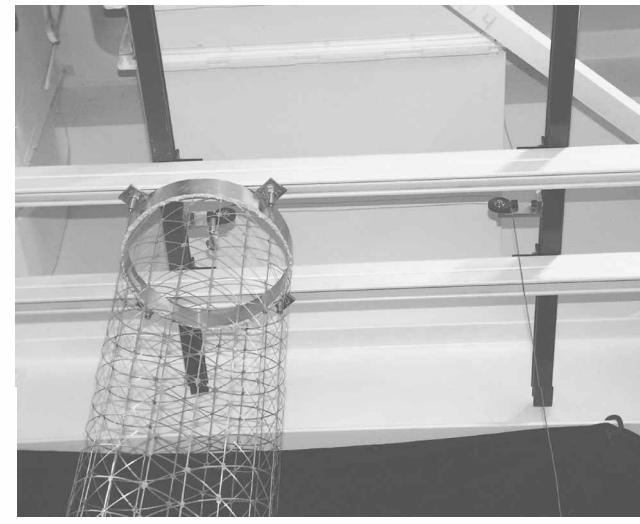

Fig. 4 Pulley alignment system.

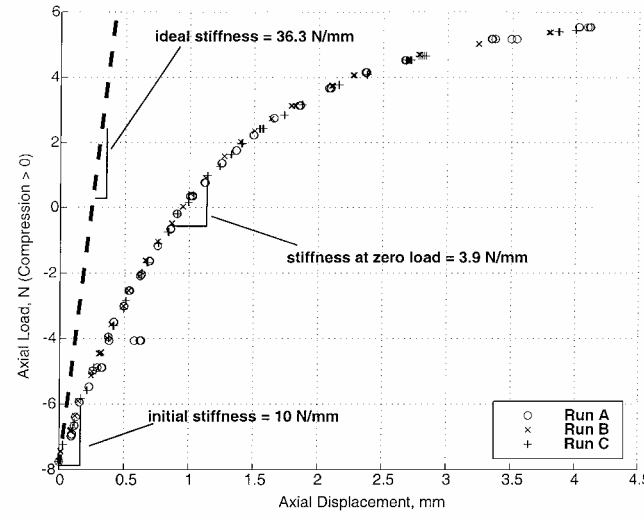

Fig. 5 Axial loading results.

Experimental Results

Axial Loading

Three axial loading sequences were performed. The loading cable was initially unloaded, resulting in an initial tension load in the test article equal to the weight of the free end fitting (7.74 N). Weights were then applied to the loading cable as described earlier, typically in 50-g increments, until the column buckled in axial compression. This sequence was repeated twice (runs A and B), and then a series of data was taken as the loading cable was unloaded (run C) to check for hysteresis in the load-displacement response.

The responses to the three axial loading sequences are shown in Fig. 5. A theoretically ideal response is also shown. The source of this prediction is described hereafter. As can be seen, the measured response was relatively repeatable and little or no hysteresis was apparent in the run C data collected during unloading. The nonlinear elastic nature of the response resembles postbuckled beam column behavior. As discussed in more detail later, this nonlinearity is attributed to the accumulated local rib and wall mechanics rather than to a global Euler buckling of the entire column.

In each test run, a local wall buckle was observed to develop throughout this response in a location near the free end fitting that possessed an observable initial imperfection before loading. A photograph of this buckling mode is shown in Fig. 6 just before failure. Note that this local buckle has a wavelength approximately equal to twice the rib spacing. Unfortunately, this local buckle corresponds

Table 1 Structural performance of thin-walled isogrid column prototype

Parameter	Ideal value	Observed value	Effective knockdown factor γ_{eff}
k_{axial}	36,300 N/m	3,900 N/m	0.11
k_{axial} (preloaded)	36,300 N/m	10,000 N/m[a]	0.28[a]
$P_{\text{cr,wall}}$ (compression)	84.5 N	6 N	0.071
k_{bending}	155 N/m	40 N/m[a]	0.26[a]
$P_{\text{cr,wall}}$ (bending)	$(\gamma 2.26 + 0.207)$ N	1.05 N[a]	0.37[a]
k_{torsion}	343 Nm/rad	0.24 Nm/rad[a]	0.0007[a]

[a]Data acquired with the column under 7.7 N of axial tensile preload.

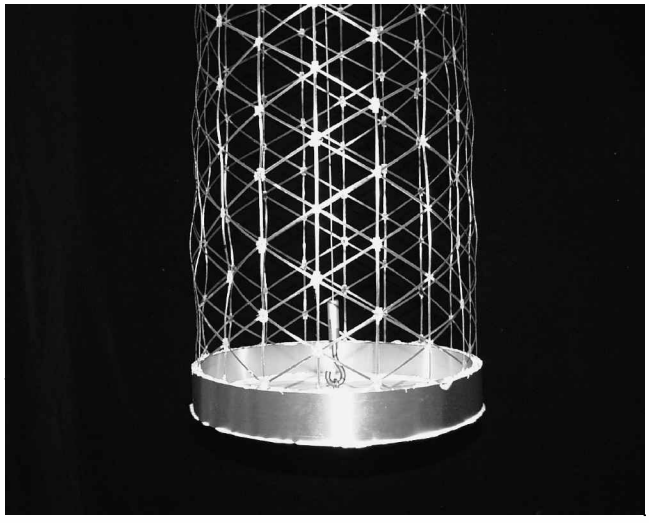

Fig. 6 Initiation of local wall buckling near free end fitting.

to prominent initial imperfections in the isogrid geometry induced by the end fitting assembly described earlier. This weak point significantly reduced the test article's ultimate axial strength. Local rib buckles were also observed to develop along the column as the buckling load was approached.

The axial loading response can be compared to an ideal model of the isogrid column derived in Ref. 3. This modeling approach initially derives equivalent isotropic material properties from the isogrid geometry and rib properties. These equivalent material properties are then combined with the larger-scale column geometry in standard thin-walled cylinder analyses. In this manner, theoretical axial, bending, and torsional stiffnesses are predicted for an imperfection-free isogrid column (k_{axial}, k_{bending}, and k_{torsion}). The theory for the buckling of thin-walled cylinders also provides estimates of the axial and bending loads, which should result in local wall buckling, $P_{\text{cr,wall}}$. The ideal and observed stiffness and strength parameters are summarized in Table 1. Also shown are the effective knockdown factors defined simply as $\gamma_{\text{eff}} \equiv k_{\text{eff}}/k_{\text{ideal}}$ and $\gamma_{\text{eff}} \equiv P_{\text{cr,eff}}/P_{\text{cr,ideal}}$. This knockdown factor approach is adopted from earlier thin-walled cylinder studies to simplify future design studies.[2]

Note that the analysis described earlier presumes classic linear elastic beam mechanics and, therefore, does not account for the observed nonlinearity found in the axial response. This nonlinearity at the equivalent material constitutive level should limit the accuracy of the subsequent bending and buckling analyses. At some point, it may be useful to consider a model of this nonlinear global behavior. However, the focus of this work is on identifying the source of performance degradation and providing quantitative specifications for improvement.

The observed axial tangential stiffness at zero column load is approximately 3900 N/m. In contrast, this value is approximately 10,000 N/m at 7 N of tensile preload. This variation indicates that imperfections present at zero load are reduced as tension is applied, resulting in increased stiffness. This stiffness would presumably approach the ideal value of 36,300 N/m if tension were further increased. The theoretically ideal axial response of the column is also indicated in Fig. 5.

As the local wall buckling mode proved to be critical in the axial testing, the observed 6-N compression capacity of the column is assumed to correspond with this failure mode. This capacity indicates an effective wall buckling knockdown factor γ_{eff} of 6/84.5, or 0.071.

This knockdown can be compared to that typically observed in monocoque cylinders. An empirically derived formula for this knockdown coefficient is discussed in Ref. 2 that captures observed dependencies of γ_{eff} on the cylinder radius-to-thickness ratio r/t as

$$\gamma_{\text{eff}} = 1 - 0.901(1 - e^{-\phi}) \tag{1}$$

where

$$\phi = \tfrac{1}{16}\sqrt{r/t} \tag{2}$$

Using the thickness of the ribs as the equivalent monocoque thickness results in a γ value of 0.26. If the isogrid material were evenly distributed, however, an equivalent thickness of $t_{\text{eq}} = 3t\,(b/h) = 0.024$ mm would result, where t, b, and h are the rib thickness, width, and spacing, respectively. Substituting this thickness rather than that of the ribs into Eqs. (1) and (2) reduces γ to 0.105.

This value then represents the typical knockdown factor in wall buckling strength for a monocoque column of equivalent mass per unit length. The similarity between this value and that observed in the test results implies that the improvement expected for an isogrid column was not demonstrated here. As will be discussed further, this result is believed to be indicative of the rib curvatures induced by the test fixturing and fabrication process rather than evidence against the potential of isogrid structures. Rather, improvements in fabricated rib straightness and test fixturing will need to be made before the benefits of the isogrid architecture can be realized.

Lateral Loading

Lateral tip loads were also applied to the column to provide additional structural performance data to compare to the ideal isogrid column model. The displacement metrology configuration was identical to that used for axial loading, but a lighter weight loading cable was configured, as shown in Fig. 7. In this configuration, the force transducer is suspended by its signal cable to prevent preloading while allowing relatively free lateral motion. The loading cable then continues through the pulley on the right, and weights were utilized as in the axial loading case.

Given the decreased stiffness and strength in bending, the load increments were reduced to 10 g. The responses to two loading sequences are shown in Fig. 8. As with the axial loading, the lateral load was increased until a local wall buckle lead to failure. This response appears to be more linear and includes a more abrupt transition to buckling than the axial loading case.

Fig. 7 Lateral loading configuration.

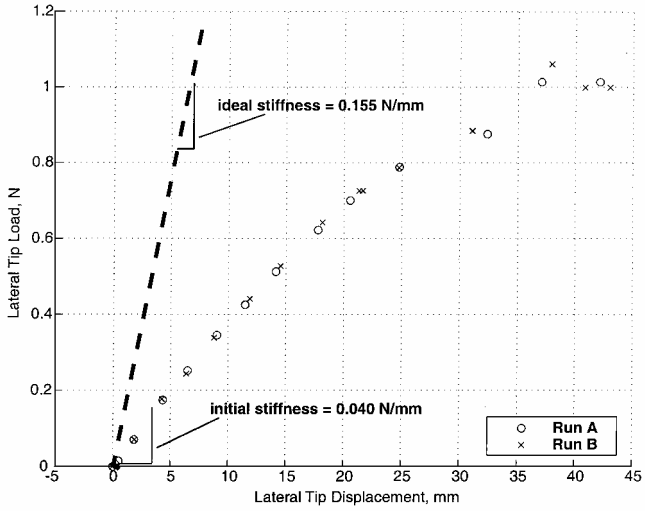

Fig. 8 Lateral loading test results.

Fig. 9 Buckling due to lateral loading.

As expected for a cantilevered beam under tip loading, the maximum stress, and, therefore, local wall buckling failure location, was near the fixed end of the column. One buckled shape due to lateral loading is shown in Fig. 9.

Again, the ideal isogrid cylindrical column model developed in Ref. 3 can be applied to analyze the results of this bending response. The ideal and observed bending stiffnesses are recorded in Table 1. Here, k_{bending} represents the stiffness of the beam column in cantilevered tip loading. As shown, the ideal cantilevered bending stiffness is 155 N/m. In comparison, the observed bending stiffness is approximately 40 N/m.

Recall the tensile preload produced by the weight of the free end fitting. Not only will this affect the expected critical lateral load, but it also appears to reduce the initial rib imperfections. As a result, the observed lateral stiffness may be somewhat greater than what would have been observed if the end fitting weight had simultaneously been off loaded. This off loading would have slightly increased the initial curvatures in the axial ribs, which would subsequently decrease bending stiffness.

This observed bending stiffness knockdown factor can also provide some indication of the effective global column buckling strength of the test article. When global imperfections are ignored, the ratio of observed and ideal bending stiffnesses is equivalent to that of effective and ideal global buckling strengths. As a result, the observed effective knockdown factor in global buckling strength would be 40/155, or 0.26.

Calculating the ideal critical wall buckling load for this bending case requires additional analysis to account for the tensile preload effects. When the equivalent isotropic material analysis of isogrid systems is utilized again, this can be accomplished with an Euler beam column analysis. When the axial and bending loads are superposed, equivalent axial stresses will be considered. For a given critical axial load, the equivalent critical axial stress for wall buckling is

$$\sigma_{\text{cr}} = \frac{P_{\text{cr,wall}}}{2\pi rt} = \gamma 417{,}000\ \text{Pa} \tag{3}$$

The axial prestress resulting from the weight of the free end fitting is 38,200 Pa. As a result, the critical stress during bending $\sigma_{\text{cr,bending}}$ must be $(\gamma 417{,}000 + 38{,}200)$ Pa to include the effect of the preload. By further application of the Bernoulli–Euler beam assumptions, the critical lateral load to induce local wall buckling at the root is expected to be

$$P_{\text{cr,bending}} = \frac{\sigma_{\text{cr,bending}} I_{\text{column}}}{L_{\text{column}} r} = (\gamma 2.26 + 0.21)\ \text{N} \tag{4}$$

With an observed $P_{\text{cr,bending}}$ of approximately 1.05 N, the effective wall buckling knockdown factor γ is found to be 0.37. This is a significant increase from the 0.071 observed value from the axial loading results.

There are at least two likely contributions to this improvement in apparent wall buckling strength. Initially, the localized initial imperfection near the free end of the column that reduced the axial loading strength did not participate in the failure during bending. Additionally, the reduction in initial rib imperfections provided by the end fitting's tensile preload would have improved the wall buckling strength.

Torsional Vibration

One last data point from the test article was obtained by measuring the first natural torsional vibration frequency. An accelerometer was attached to the free end fitting as shown in Fig. 10. The accelerometer was oriented roughly orthogonal to the column radius and axis.

A static torsional load was manually applied to the free end of the column and then released. The resulting accelerometer signal was recorded on an oscilloscope and indicated a natural vibration frequency of 3.6 Hz.

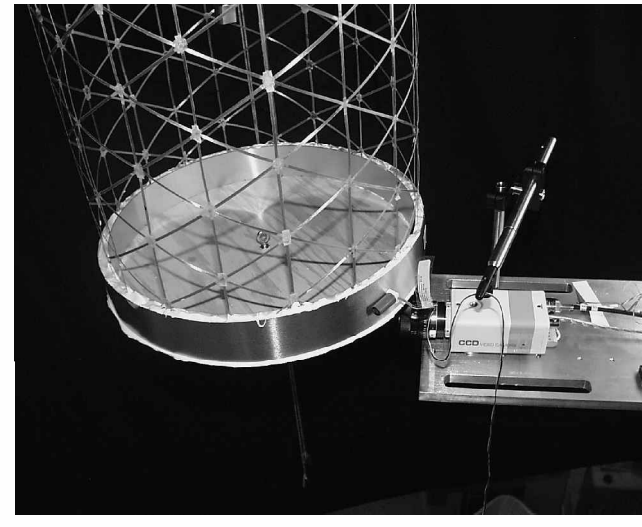

Fig. 10 Accelerometer configuration for torsional vibration testing.

The ideal torsional stiffness as modeled in Ref. 3 is 343 Nm/rad. The observed vibration frequency can be related to the effective torsional stiffness according to $k_{\text{torsion,eff}} = J_{\text{end}} f^2$.

The radius of gyration of the 0.79-kg free end fitting is approximately 0.152 m. The resulting rotational inertia of the end fitting is 0.018 kg · m^2. Therefore the 3.6-rad/s mode corresponded to a torsional stiffness of 0.24 Nm/rad. This is over three orders of magnitude lower than the ideal torsional stiffness.

The column's ideal torsional stiffness is derived primarily from axial loading of the diagonal or ±60-deg ribs. The global torsional loads induce shear in the isogrid wall of the column. The isogrid's diagonal ribs play a similar role to the cross bracing of a more common truss beam, translating global shear loads into axial loads in these elements. However, because the prototype was fabricated on a cylindrical mandrel, all of the diagonal ribs possess an initial bow of approximately 2.4 mm. As a result, these ribs are forced to carry significant bending loads while the column is in torsion. As will be discussed in the following sections, the resulting decrease in rib stiffness provides an explanation for the significantly diminished torsional stiffness.

Summary of Experimental Results

In summary, the measured stiffness and strength of the test article exhibits large knockdown factors from models assuming an ideal isogrid geometry. This knockdown is particularly severe in the case of torsional stiffness with the measured result having less than 0.1% of the ideal case. These knockdowns appear to be due to initial curvatures of the isogrid ribs due to the fabrication and test fixturing processes. The following section derives a relationship between local rib curvatures and the global structural characteristics and compares the predictions to the observed values.

Geometric Imperfections Analysis

The strong sensitivity of the test article's stiffness and strength to local imperfections will be examined in this section. Although a number of physical and geometric imperfections are present in any structure, the effects of initial rib curvatures were found to dominate the response of the isogrid column prototype. The objective here is to develop analytical tools that allow the impact of initial rib curvatures on the global response of these structures to be accurately predicted. This approach represents an alternative to the empirical equations developed for monocoque shells in the prediction of imperfection knockdown factors.[2] As a result, the analysis will allow for more informed specifications in the fabrication process and may suggest improved architectures for reducing the sensitivity of the global performance to local imperfections.

Rib Curvature and Axial Stiffness Relationship

The approach proposed here is to treat the effect of initial rib curvatures as knockdowns in the isogrid's equivalent isotropic material modulus. As a result, the typical truss mechanics assumption of predominantly axial load transmission in individual members/ribs is being applied. Note that this assumption will be less accurate as rib curvatures become large relative to their thickness.

The ribs are modeled as axially loaded beam columns with an initial half-sine imperfection. The axial shortening of such a system was shown in Ref. 10 to be

$$\delta = \frac{PL}{AE} + \varepsilon^2\left[\frac{\pi^2}{4L(1-q)^2} - \frac{\pi^2}{4L}\right] \tag{5}$$

where ε is the imperfection amplitude and q is the ratio of the applied load to the buckling load given by

$$q = PL^2/\pi^2 EI \tag{6}$$

The tangential compliance of this system at zero load will be derived and compared to that for $\varepsilon = 0$ to determine an effective stiffness knockdown as a function of ε. When Eqs. (5) and (6) are combined,

$$\delta = PL/AE + (\varepsilon^2\pi^2/4L)(1 - PL^2/\pi^2 EI)^{-2} - \varepsilon^2\pi^2/4L \tag{7}$$

The compliance is then

$$c_{\text{eff}} = \frac{\partial\delta}{\partial P} = \frac{L}{AE} + \frac{\varepsilon^2 L}{2EI}\left(1 - \frac{PL^2}{\pi^2 EI}\right)^{-3} \tag{8}$$

and the initial compliance at $P = 0$ is

$$c_{\text{eff}} = \frac{\partial\delta}{\partial P}_{P\to 0} = \frac{L}{AE} + \frac{\varepsilon^2 L}{2EI} \tag{9}$$

The effective axial stiffness knockdown will be defined as

$$\gamma_{\text{rib}} = \frac{c_{\text{ideal}}}{c_{\text{eff}}} = \frac{L/AE}{L/AE + \varepsilon^2 L/2EI} = \frac{1}{1 + \varepsilon^2 A/2I} \tag{10}$$

For the rectangular rib geometry, $A = bt$ and $I = bt^3/12$. This further reduces Eq. (10) to

$$\gamma_{\text{rib}} = 1/[1 + 6(\varepsilon/t)^2] \tag{11}$$

A plot of γ_{rib} vs ε/t is shown in Fig. 11. This indicates the sensitivity of the axial stiffness of the ribs to their initial curvature magnitude. In general, as ε/t proceeds from 0.1 to 1, there is a rapid loss of stiffness. It was noted in Ref. 9 that postbuckling stiffness eventually approaches that of a cantilevered beam with a lateral rather than axial load for extremely large curvatures.

Rib Imperfections and Column Performance Relationships

It is further assumed that this effective axial rib stiffness knockdown will have a proportional impact on the isogrid's equivalent isotropic material modulus. Each ideal stiffness and strength parameter is, in turn, proportional to this modulus and, therefore, the axial rib stiffness knockdown factor. As a result, setting γ_{rib} equal to the γ_{eff} values presented in Table 1 should indicate an effective amount of rib curvature ε/t for each parameter.

When Eq. (11) is solved for ε/t,

$$\varepsilon/t = \sqrt{(1 - \gamma_{\text{rib}})/6\gamma_{\text{rib}}} \tag{12}$$

The equivalent rib curvature amplitudes that correspond to the effective knockdown factors in Table 1 can now be calculated and are listed in Table 2. Also recorded in Table 2 are the ribs that were the

Table 2 Equivalent initial rib curvatures

Parameter	Effective knockdown factor $\gamma_{\text{eff}} = \gamma_{\text{rib}}$	Equivalent rib curvature ε, mm	Participating ribs
k_{axial}	0.11	0.24	Axial
k_{axial} (preloaded)	0.28[a]	0.13	Axial
$P_{\text{cr,wall}}$ (compression)	0.071	0.3	Localized axial
k_{bending}	0.26[a]	0.14	Axial
$P_{\text{cr,wall}}$ (bending)	0.37[a]	0.11	Localized axial
k_{torsion}	0.0007[a]	3.1	Diagonal

[a]Data acquired with the column under 7.7 N of axial tensile preload.

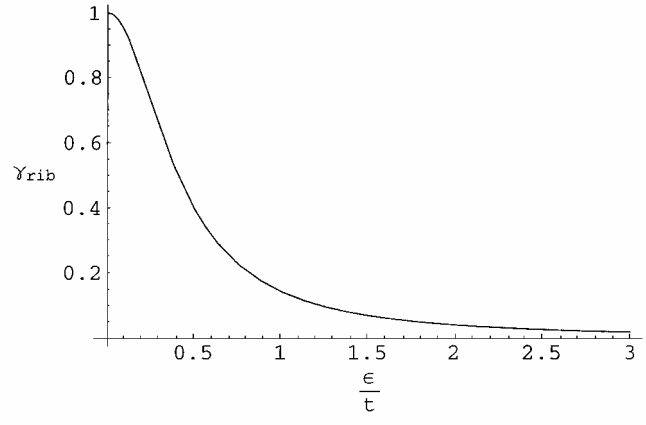

Fig. 11 Sensitivity of rib axial stiffness to initial curvature magnitude.

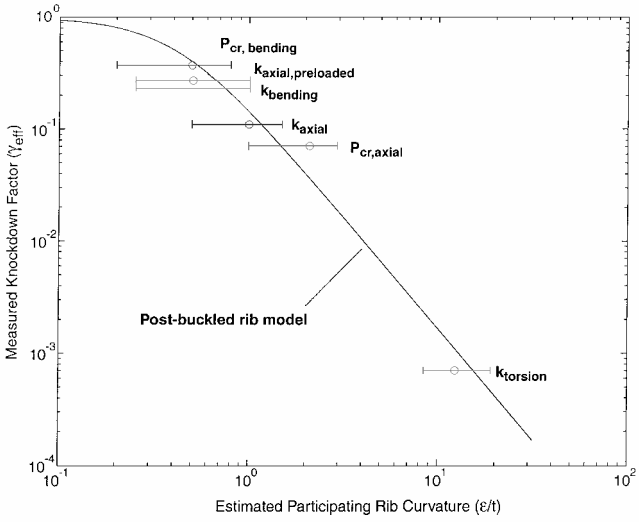

Fig. 12 Theoretical and observed relationship between rib curvatures and knockdown factors.

primary participants in each loading case. As described earlier, each stiffness and strength parameter possesses varying dependencies on the magnitudes and distribution of initial rib imperfections. These variations are indicated in the results in Table 2.

Visual measurements of the axial and diagonal rib curvatures were made to compare with these predictions. The axial ribs in the prototype possess equivalent rib curvatures near or less than the 0.2-mm rib thickness, with localized exceptions appearing as large as 1 mm. As described earlier, the axial tensile preload applied by the free end fitting's weight was observed to straighten these ribs significantly, thereby improving their stiffness contributions. The diagonal ribs, however, each possess a significant amount of curvature due to the fabrication technique. As described in the earlier torsional vibration analysis, this initial curvature of the diagonal ribs is approximately 2.4 mm in amplitude due to the cylindrical mandrel the component was constructed on.

These rib curvature values are combined with the corresponding observed knockdowns and compared with the postbuckled rib model in Fig. 12 to allow the accuracy of the model to be assessed. A logarithmic plot of the data allows the details across the entire range of knockdown factors to be observed. Also indicated are the 95% confidence bounds in the rib curvature measurements.

When these results are inspected, the impact of the wide range of rib curvatures in the prototype can be observed. In general, the strongly nonlinear relationship between rib curvature and knockdown factors observed in the test data is well accounted for by the postbuckled rib model. At one extreme of Fig. 12, the torsional stiffness knockdown factor of 0.007 due to the consistently large curvature in the diagonal ribs follows that predicted by the model within the precision of the curvature measurements. Reasonable agreement is also found for the lower rib curvatures typical of the axially preloaded cases of bending stiffness and strength, as well as the initial axial stiffness. The slight increase in axial rib curvature that was observed as the axial preload was removed is found to account for the observed corresponding decrease in axial stiffness. Finally, the larger initial localized curvatures at the point of failure in the axial tests resulted in a further decrease in axial buckling strength.

Conclusions

The objectives of this study were to determine the stiffness and strength of the prototype gossamer column and to assess the accuracy of existing open isogrid column models. In general, the measured stiffness and strength of the test article exhibits severe knockdown factors from models when an ideal isogrid geometry is assumed. This performance decrease is particularly excessive in the case of torsional stiffness with the measured performance less than 0.1% of the ideal case. These knockdown factors appear to be due to initial curvatures of the isogrid ribs caused by the fabrication and test fixturing processes.

This motivated the development of a model of the global effect of initial individual rib curvatures. A strongly nonlinear relationship between initial rib curvature and axial stiffness is indicated by the Euler beam column analysis of postbuckling behavior. In general, it is predicted that local curvature amplitudes greater than 10% of the rib thickness result in a rapid degradation of axial stiffness. The equivalent modulus of the isogrid is assumed to vary in proportion to these axial rib knockdown factors to relate them to the global performance of the column.

The observed knockdown factors and rib curvatures are found to be well correlated with this model. The global impact of variations in rib curvature between the axial and diagonal ribs is accurately predicted. Also, the effect of reduced rib curvatures due to axial preloading is well represented. Finally, both stiffness and strength performance variations are captured. As a result, the equivalent modulus knockdown approach appears to provide a useful prediction of the effects of both localized and homogeneous rib imperfections on the global column response. This tool will be particularly useful in specifying geometric tolerances for the fabrication of future isogrid components.

Acknowledgments

This research was sponsored by the NASA Langley Research Center through the Small Business Innovation Research Program under Contract NAS1-00034. The Technical Monitor was Timothy J. Collins. Special thanks go to Mark S. Lake and Martin M. Mikulas for their technical input.

References

[1]Gefert, L. P., Hack, K. J., and Kerslake, T. W., "Options for the Human Exploration of Mars Using Solar Electric Propulsion," *Space Technology and Applications International Forum 1999, American Institute of Physics Conference Proceedings 458*, American Inst. of Physics, 1999, p. 1275.

[2]Weingarten, V. I., Seide, P., and Peterson, J. P., "Buckling of Thin-Walled Circular Cylinders," NASA SP-8007, Sept. 1965.

[3]Mikulas, M. M., Jr., "Structural Efficiency of Long Lightly Loaded Truss and Isogrid Columns for Space Applications," NASA TM 78687, July 1978.

[4]*Isogrid Design Handbook*, NASA CR-124075, Feb. 1973.

[5]Forman, S. E., and Hutchinson, J. W., "Buckling of Reticulated Shell Structures," *International Journal of Solids and Structures*, Vol. 6, No. 7, 1970, pp. 909–932.

[6]Anderson, M. S., "Buckling of Periodic Lattice Structures," *AIAA Journal*, Vol. 19, No. 6, 1980, pp. 782–788.

[7]Anderson, M. S., "Buckling of Imperfect Periodic Lattice Structures," *Collapse: The Buckling of Structures in Theory and Practice*, edited by J. M. T. Thompson and G. W. Hunt, Cambridge Univ. Press, Cambridge, England, U.K., 1982, pp. 209–219.

[8]Anderson, M. S., "Nonlinear and Tangent Stiffness of Imperfect Beam Columns," NASA TM 84497, Dec. 1982.

[9]Fichter, W. B., and Pinson, M. W., "Load-Shortening Behavior of an Initially Curved Eccentrically Loaded Column," NASA TM 101643, 1989.

[10]Lake, M. S., and Georgiadis, N., "Analysis and Testing of Axial Compression in Imperfect Slender Truss Struts," NASA TM 4174, Feb. 1990.

[11]Roorda, J., "Some Statistical Aspects of the Buckling of Imperfection-Sensitive Structures," *Journal of the Mechanics and Physics of Solids*, Vol. 17, No. 2, 1969, pp. 111–123.

[12]Crawford, R. F., and Hedgepeth, J. M., "Effects of Initial Waviness on the Strength and Design of Built-up Structures," *AIAA Journal*, Vol. 13, No. 5, 1975, pp. 672–675.

[13]Rosen, A., and Schmit, L. A., Jr., "Design-Oriented Analysis of Imperfect Truss Structures—Part 1—Accurate Analysis," *International Journal for Numerical Methods in Engineering*, Vol. 14, No. 9, 1979, pp. 1309–1321.

[14]Hinkle, J. D., and Peterson, L. D., "A Micron-Precision Metrology System for Measuring Structural Geometric Repeatability," M.S. Thesis, Dept. of Aerospace Engineering Sciences, Univ. of Colorado, Boulder, CO, May 1995.

J. Lassiter
Guest Editor